Spectrochimica Acta Part A: Molecular and Biomolecular Spectroscopy 268 (2022) 120662

Contents lists available at ScienceDirect

Spectrochimica Acta Part A: Molecular and Biomolecular Spectroscopy

journal homepage: www.elsevier.com/locate/saa

Comparison of rhodamine 6G, rhodamine B and rhodamine 101 spirolactam based fluorescent probes: A case of pH detection

Fei Deng [a,*], Dongsheng Sun [b], Shixu Yang [a], Wei Huang [a], Chunfang Huang [a], Zhaochao Xu [c,*], Limin Liu [a,*]

[a] School of Chemistry and Chemical Engineering, Jinggangshan University, Ji'an, Jiangxi 343009, China
[b] School of Medicine, Taizhou University, Taizhou, Zhejiang 318000, China
[c] CAS Key Laboratory of Separation Science for Analytical Chemistry, Dalian Institute of Chemical Physics, Chinese Academy of Sciences, Dalian 116023, China

HIGHLIGHTS

- Spirolactam based pH probes (**RLH A-C**) were built with Rhodamine 6G, Rhodamine B and Rhodamine 101 to discuss the tuning effect of rhodamine fluorophore.
- The pK_a values and observed rate constant k_{obs} of **RLH A-C** were determined and found to negatively correlated with the calculated Gibbs free energy differences $\Delta G_{C\text{-}O}$ and ΔG_{TS} respectively.
- The pK_a values and observed rate constant k_{obs} of **RLH A-C** determined the potential application in intracellular pH detection.

GRAPHICAL ABSTRACT

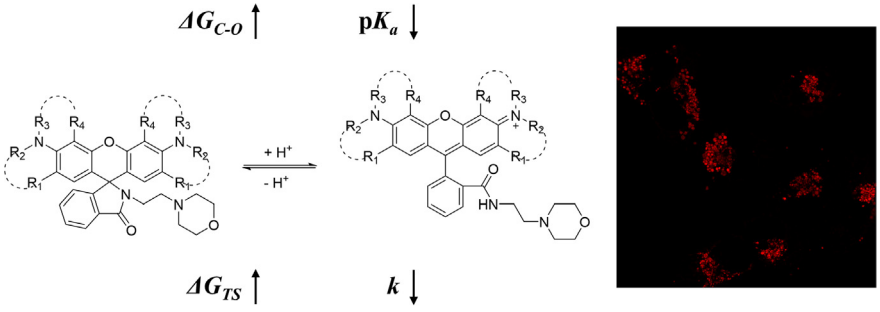

ARTICLE INFO

Article history:
Received 13 September 2021
Received in revised form 15 November 2021
Accepted 23 November 2021
Available online 26 November 2021

Keywords:
Rhodamine
Spirolactam
Fluorescent probe
pH

ABSTRACT

Ring-opening reaction of rhodamine spirolactam has been widely applied to construct fluorescent probes. The fluorescence properties of the probe were finely tuned for specific purpose through changing the rhodamine fluorophore. However, the influence on response range and kinetic parameters of the probe during the change has been seldom discussed. Herein, we took pH detection as an example and constructed spirolactam based probes (**RLH A-C**) with Rhodamine 6G, Rhodamine B and Rhodamine 101. The pK_a values and observed rate constant k_{obs} of **RLH A-C** were determined and found to negatively correlated with the calculated Gibbs free energy differences $\Delta G_{C\text{-}O}$ and ΔG_{TS} respectively. The potential applications of **RLH A-C** in imaging acidic microenvironment were also investigated in cells. We expect the comparison of rhodamine fluorophores will facilitate the quantitative optimization of rhodamine spirolactam based fluorescent probes.

1. Introduction

Fluorescent probe has been widely used as a tool in life science, for example, directly observing dynamics of bioactive molecules in cellular physiological processes [1,2]. Any phenomenon that results in a change of fluorescence intensity [3], wavelength [4] or lifetime [5] can be used for the analysis process. The general and valuable mechanisms of fluorescence change during detection including intermolecular charge transfer (ICT), photoinduced electron transfer (PET) and fluorescence resonance energy transfer (FRET) [6,7]. Lots of fluorescent probes have been developed based on these mechanisms, such as probes for detecting Ca^{2+}, GSH [8,9]. Besides, some switch structures were also applied in designing fluorescent probes. Czarnik's group reported the first rhodamine

* Corresponding authors.
E-mail addresses: dengfei@jgsu.edu.cn (F. Deng), zcxu@dicp.ac.cn (Z. Xu), llm24@126.com (L. Liu).

https://doi.org/10.1016/j.saa.2021.120662
1386-1425/

spirolactam based fluorescent probe in 1997 [10]. The ring-opening reaction of Rhodamine B hydrazide was triggered by Cu^{2+} with the transformation from nonfluorescent spirolactam structure to fluorescent ion structure. Inspired by this pioneering work, ring-opening strategy was further extended to other chemical species detection with the change of groups linked to nitrogen atom in spirolactam structure [11–13].

Since rhodamine xanthene ring did not participate the binding of analytic objects in sensing, the choice of rhodamine fluorophore was rarely considered in fluorescent probe designing. Most of the spirolactam structures were constructed directly from the commercially available Rhodamine B [14], Rhodamine 6G [15] or Rhodamine 101 [16]. Through replacing the fluorophores to hybrid rhodamine, some of the fluorescent probes were further extended for special fluorescence properties, including near-infrared emission or large-stokes shift [17–20]. The data from different reports indicated rhodamine fluorophores greatly influenced the response range and kinetic parameters of the fluorescent probes [21–23]. Particularly, some of the analogues could hardly recognize target via similar mechanism compared to their parent fluorescent probes [24]. Therefore, systematically comparison of spirolactam structures with different rhodamine fluorophores were beneficial for the quantitative design of fluorescent probes. Unfortunately, few works focused on this problem, especially the comparison of common commercially available rhodamines.

Rhodamine spirolactam, as the pH sensitive structure, has often been applied to detecting pH. Recently, Zhang et al. reported a rhodamine B lactam derivative with morpholine as a lysosome tracker [25]. The probe showed a 140-fold fluorescence enhancement over a pH range from 7.4 to 4.5 and could monitor the lysosomal pH. Replacing rhodamine B fluorophore of the probe to near-infrared rhodamine and hemicyanine rhodamine could also sense the pH change [26,27]. In this paper, we took the morpholine contained spirolactam structure as an example to illustrate the tuning effect of rhodamine fluorophore. Three pH probes based on rhodamine 6G, rhodamine B and rhodamine 101 were synthesized. The optical and chemical properties of these probes were substantiated with theoretical calculations. Besides, these probes were also applied to imaging the lysosomal pH.

2. Experimental section

2.1. Materials and instruments

Unless otherwise stated, all reagents and solvents for synthesis and detection were purchased from commercial suppliers and used without further purification. All water used was from Millipore water purification system with a minimum resistivity of 18.0 MΩ·cm. ^{1}H NMR and ^{13}C NMR spectra were recorded on a Bruker 400 spectrometer, using tetramethylsilane (TMS) as an internal standard. Chemical shifts were given in ppm and coupling constants (J) in Hz. Mass spectrometry data were obtained with Waters Xevo G2-XS QTof. UV–Vis absorption spectra were collected on Shimadzu UV-1900i Spectrophotometer. Fluorescence measurements were performed on PerkinElmer LS55 fluorescence spectrophotometer. The fluorescence imaging was performed by using Olympus FV1000 MPE confocal laser scanning microscope.

2.2. Synthesis

Compound **1**: This compound was synthesized according to the literature [28]. ^{1}H NMR (400 MHz, DMSO d_6) δ 7.96 (dt, J = 7.5, 1.1 Hz, 1H), 7.76 (td, J = 7.4, 1.2 Hz, 1H), 7.68 (td, J = 7.4, 1.0 Hz, 1H), 7.18 (dt, J = 7.7, 1.0 Hz, 1H), 6.33 (s, 2H), 6.21 (s, 2H), 5.27 (t, J = 5.5 Hz, 2H), 3.27 – 3.09 (m, 4H), 1.90 (s, 6H), 1.21 (t, J = 7.1 Hz, 6H).

General Procedure for Synthesis of **RLH A-C**: The corresponding rhodamine (1.0 mmol), 4-(2-aminoethyl) morpholine (3.0 mmol) and benzotriazol-1-yl-oxytripyrrolidinophosphonium hexafluorophosphate (PyBop, 1.1 mmol) were dissolved in 25 mL CH_2Cl_2. The mixture was stirred for 12 h at room temperature before evaporated under reduced pressure. The crude product was purified by column chromatography (EtOAc/PE = 3:2) to afford pure product. **RLH A**: 86.7%; ^{1}H NMR (400 MHz, $CDCl_3$) δ 7.93 (d, J = 6.8 Hz, 1H), 7.57 – 7.41 (m, 2H), 7.05 (d, J = 6.7 Hz, 1H), 6.35 (s, 2H), 6.26 (s, 2H), 3.63 – 3.46 (m, 6H), 3.25 (dt, J = 15.2, 5.2 Hz, 6H), 2.26 (s, 4H), 2.15 – 2.02 (m, 2H), 1.91 (s, 6H), 1.34 (t, J = 7.1 Hz, 6H); ^{13}C NMR (100 MHz, $CDCl_3$) δ 168.13, 153.68, 151.70, 147.37, 132.37, 131.16, 128.69, 127.99, 123.75, 122.72, 117.76, 106.10, 96.45, 66.90, 64.94, 56.03, 53.16, 38.38, 36.85, 16.71, 14.74; ESI-HRMS calcd. for $C_{32}H_{38}N_4O_3$ $[M + H]^+$ 527.3022, observed 527.3021. **RLH B**: 89.5%; ^{1}H NMR (400 MHz, $CDCl_3$) δ 7.91 (dd, J = 5.7, 3.0 Hz, 1H), 7.45 (dd, J = 5.7, 3.1 Hz, 2H), 7.10 (dd, J = 5.6, 3.0 Hz, 1H), 6.45 (d, J = 8.8 Hz, 2H), 6.39 (d, J = 2.6 Hz, 2H), 6.27 (dd, J = 8.8, 2.6 Hz, 2H), 3.59 (t, J = 4.6 Hz, 4H), 3.40 – 3.26 (m, 10*H*), 2.27 (t, J = 4.6 Hz, 4H), 2.12 (t, J = 7.5 Hz, 2H), 1.17 (t, J = 7.0 Hz, 12H); ^{13}C NMR (100 MHz, $CDCl_3$) δ 167.94, 153.47, 153.34, 148.72, 132.29, 131.34, 129.06, 127.99, 123.77, 122.68, 108.04, 105.66, 97.68, 66.88, 64.83, 56.07, 53.22, 44.39, 36.96, 12.59; ESI-HRMS calcd. for $C_{34}H_{42}N_4O_3$ $[M + H]^+$ 555.3335, observed 555.3333. **RLH C**: 56.3%; ^{1}H NMR (400 MHz, $CDCl_3$) δ 7.90 (dd, J = 5.5, 3.1 Hz, 1H), 7.51 – 7.36 (m, 2H), 7.10 (dd, J = 5.6, 2.9 Hz, 1H), 6.01 (s, 2H), 3.62 (t, J = 4.7 Hz, 4H), 3.31 – 3.02 (m, 10H), 2.90 (t, J = 6.7 Hz, 4H), 2.48 (t, J = 6.5 Hz, 4H), 2.38 – 2.25 (m, 4H), 2.08 (ddt, J = 17.7, 12.1, 6.9 Hz, 6H), 1.95 – 1.81 (m, 4H); ^{13}C NMR (100 MHz, $CDCl_3$) δ 167.99, 153.68, 148.31, 143.52, 132.24, 131.30, 127.81, 124.88, 123.91, 122.58, 117.18, 107.56, 105.77, 66.89, 65.66, 56.07, 53.22, 49.94, 49.49, 36.88, 27.19, 22.05, 21.55, 21.24; ESI-HRMS calcd. for $C_{38}H_{42}N_4O_3$ $[M + H]^+$ 603.3335, observed 603.3331.

2.3. Sample preparation

RLH A-C were dissolved in DMSO to afford 2.0 mM stock solution. The stock solution was diluted to 5 μM with Britton-Robison (BR) buffer solution for absorbance and fluorescence measurements. Except for kinetic analysis, the test samples were incubated for 30 min at room temperature before measurements.

2.4. Determination of pK_a and kinetic parameters

pK_a of **RLH A-C** was obtained by using the equation below:

$$F = \frac{F_{max} + F_{min} \times 10^{pH-pK_a}}{1 + 10^{pH-pK_a}}$$

Time-dependent fluorescence change of **RLH A-C** was fitted on the following equation:

$$F = F_\infty + Ae^{-k_{obs}(t-t_0)}$$

where k_{obs} is the observed rate constant.

The observed half-life $t_{1/2}$ can be defined as follows:

$$t_{1/2} = \frac{ln2}{k_{obs}}$$

2.5. Computational details

The starting structures of **RLH A-C** and their protonated versions were obtained using Avogadro with UFF minimization of

energies. The ground and transient states geometric optimizations were then performed at r^{2}SCAN-3c composite method [29] using ORCA 5.0.0 [30–32]. Single point energies of these optimized structures were further calculated using RI-ωB97M-V/def2-TZVP. The calculated Gibbs free energy differences were corrected by subtracting the calculated absolute hydration free energy [33]. The excited states were assessed on TDDFT RI-PBE0/def2-SV(P). All calculation were conducted in the CPCM solvation model of water. The corresponding electrostatic potential, absorption and emission were analyzed by Multiwfn [34]. Molecular representations were conducted by VMD [35] and Avogadro [36].

2.6. Cell culture and imaging experiments

HuH-7 cells were cultured in Dulbecco's modified Eagle's medium (DMEM) containing 10% fetal bovine serum (FBS) under standard culture conditions (atmosphere of 5% CO_2 and 95% air at 37 °C) for 48 h before imaging. The cells were then rinsed twice with PBS and incubated with **RLH A-C** (5 μM) and Hoechst 33342 (0.5 μg/mL) in serum free DMEM for 15 min. After incubation, cells were rinsed with PBS twice again for imaging.

3. Results and discussions

3.1. Probe design and synthesis

Spirolactam contained probes **RLH A-C** were constructed from commercially available rhodamine 6G, rhodamine B and rhodamine 101 with the link of morpholine. As illustrated in scheme 1, rhodamine 6G were hydrolyzed in KOH solution to afford compound **1**. The carboxylic acid residue in compound **1**, rhodamine B and rhodamine 101 reacted with 4-(2-aminoethyl) morpholine in the presence of PyBOP reagent to afford **RLH A-C** respectively. The final structures of **RLH A-C** were characterized by ^{1}H NMR, ^{13}C NMR, and HRMS.

3.2. Spectroscopic responses to pH

We examined the absorption and emission spectra of **RLH A-C** in BR buffers containing 0.25% DMSO at different pH. As depicted in Fig. 1a, **RLH A** exhibited almost no absorption above 400 nm at neutral and basic pH environments. When the pH decreased from 6.08 to 2.55, the gradually enhanced peak at 530 nm indicated the transformation of **RLH A** from colorless ring-colsed spirolactam to pink ring-opening ion. When pH varied from 6.08 to 2.55, the emission maxima of **RLH A** in 551 nm increased, in agreement with the absorption changes (Fig. 1b). The baseline drifts of **RLH B** absorption at neutral and basic pH environments were similar to our previous report in Si-rhodamine [37]. We attributed this phenomenon to the aggregation of **RLH B**. Gradual decreases in the pH from 5.91 to 4.00 result in the ease of baseline drifts and increase of absorption peak in 561 nm (Fig. 1c). The fluorescence spectra of **RLH B** in Fig. 1d showed the emission maxima increase in 581 nm with the pH decrease from 5.91 to 4.00. **RLH C** displays no absorption from 450 nm to 650 nm and maintains a ring-closed spirolactam structure under basic pH. A stepwise decrease in pH value from 7.40 to 3.10 leads to a new absorption peak at 584 nm with corresponding increases in the intensity (Fig. 1e). Similar to absorption, the fluorescence with peak of 602 nm gradually increased due to significantly enhanced π-conjugation as the spirolactam ring opens under acidic conditions (Fig. 1f).

3.3. pK_a and kinetic parameters

The pK_a values for **RLH A-C** were determined as 3.92, 5.00 and 5.57 respectively via pH titration of fluorescence intensity at their emission maxima (Table 1 and Fig. 2a). These comparative results indicate the response range of spirolactam structure to pH were rhodamine fluorophore dependent. Considering the intracellular acidic lysosomes pH values from 4.0 to 5.5, the pK_a values of **RLH A-C** were suitable for lysosomal pH tracking.

To further study practical applications of **RLH A-C**, we proceeded to investigate the kinetics of these probes. Time courses of fluorescence intensity at emission maxima were examined in BR solution (pH 4.00). Notably, **RLH C** responded the most rapidly

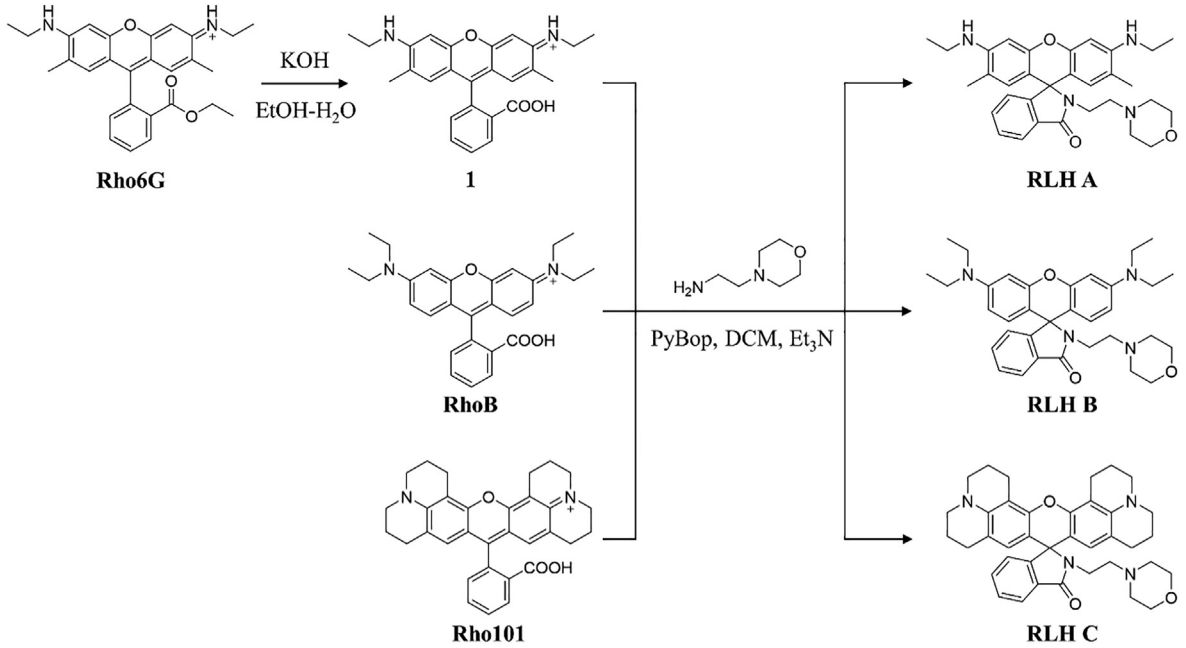

Scheme 1. Synthesis of **RLH A-C**.

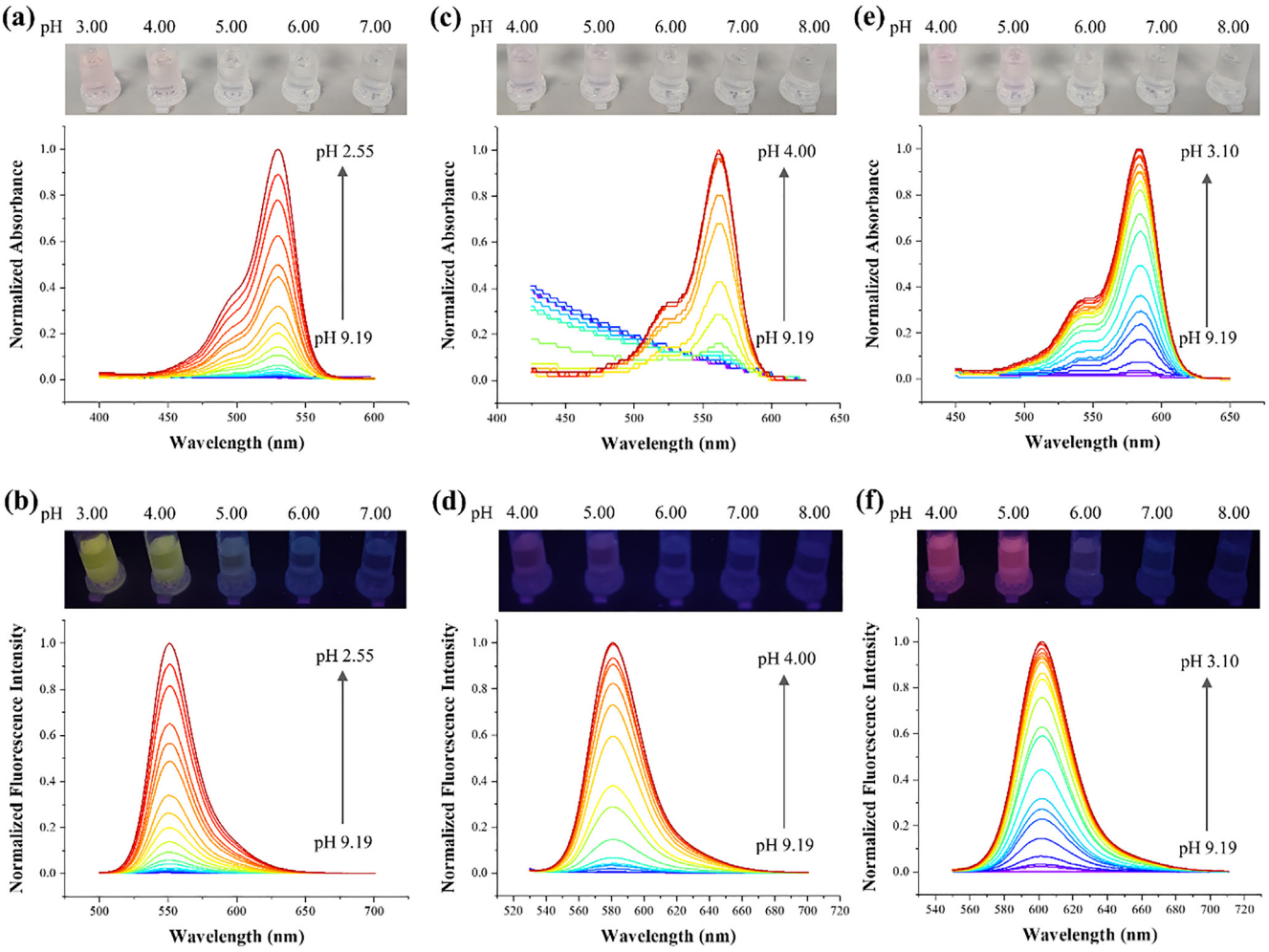

Fig. 1. Absorption and fluorescence spectra of 5 μM **RLH A** (a, b), **RLH B** (c, d) and **RLH C** (e, f) in BR solution with different pH. (Insets: photographs of the representative probe solution under daylight or 365 nm UV light. Note: photograph in 1f contain the fluorescence (400–550 nm) from julolidine structure of ring-closed **RLH C**.)

Table 1
The pK_a, kinetic parameters and calculated Gibbs free energy differences of **RLH A-C.**

Probe	pK_a	k_{obs} [s^{-1}]	$T_{1/2}$ [s]	$\Delta G_{C\text{-}O}$ [eV]	ΔG_{TS} [eV]
RLH A	3.92	0.0057	121.60	−0.0417	0.5143
RLH B	5.00	0.0047	147.48	−0.3743	0.5850
RLH C	5.57	0.0250	27.73	−0.4952	0.4890

to protons and fluorescence intensity saturation reached in a short time (within 200 s). The ring-opening reaction of **RLH A** and **RLH B** were much slower with the saturation time about 800 s. The calculated kinetic parameters of these probes were summarized in Table 1.

3.4. Selectivity to pH

To explore the practical application of these probes, the selectivities of **RLH A-C** to protons were investigated with fluorescence responses at pH 7.40 and 4.00. As shown in Fig. 3, the presence of 50 μM cations such as Na^+, K^+, Ca^{2+}, Mg^{2+}, Cd^{2+}, Co^{2+}, Ni^{2+}, Zn^{2+}, Cu^{2+}, Fe^{3+}, or anions such as Ac^-, NO^{3-}, SO_3^{2-}, CO_3^{2-} showed negligible influence to the probes in pH 7.40 or 4.00. In addition, the fluorescence intensity of **RLH A-C** in pH 7.40 and 4.00 remained stable upon addition of common amino acids and biothiols such as Cys, Ser, Arg, Met, Lys, Thr, Leu, Trp, Glu, His, Asp and GSH. These results demonstrated that **RLH A-C** were highly selective to detect acidic pH even in complicated biological environment. Besides single interferent, we also investigated the selectivity of the probes to pH over complex interferents. The addition of interferences mentioned above (without SO_3^{2-}; SO_4^{2-}; HS^-; HCO_3^- and CO_3^{2-} for stable solution) at the same time did not affect the selectivity to pH (Fig. S12).

3.5. Computational analysis

In order to verify the pK_a and kinetic difference between **RLH A-C**, we conducted theoretical studies (geometry optimization, electrostatic potential, single point energy and TD-DFT calculations) using ORCA 5.0.0. The oxygen of carbonyl group has the most negative electrostatic potential in **RLH A-C**, which benefit the binding of proton at the primary of the ring-opening reaction (Fig. 4a, S13, S17, S21, Tables S8, S9, S17, S18, S26 and S27). Although the morpholine group might bind another proton and form the two positive charged structure [25,26], we ignored this possibility to

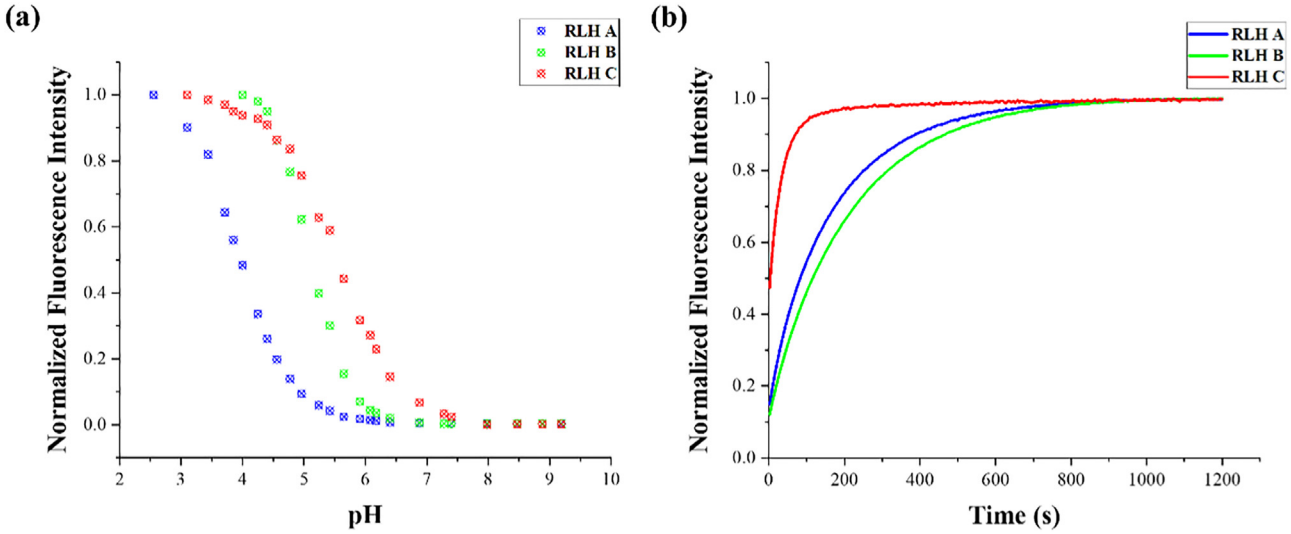

Fig. 2. (a) pH titration curves of **RLH A-C** (5 μM) at λ_{max} in BR solution; (b) Time-dependent fluorescence change of **RLH A-C** (5 μM) at the λ_{max} in pH 4.00 BR solution.

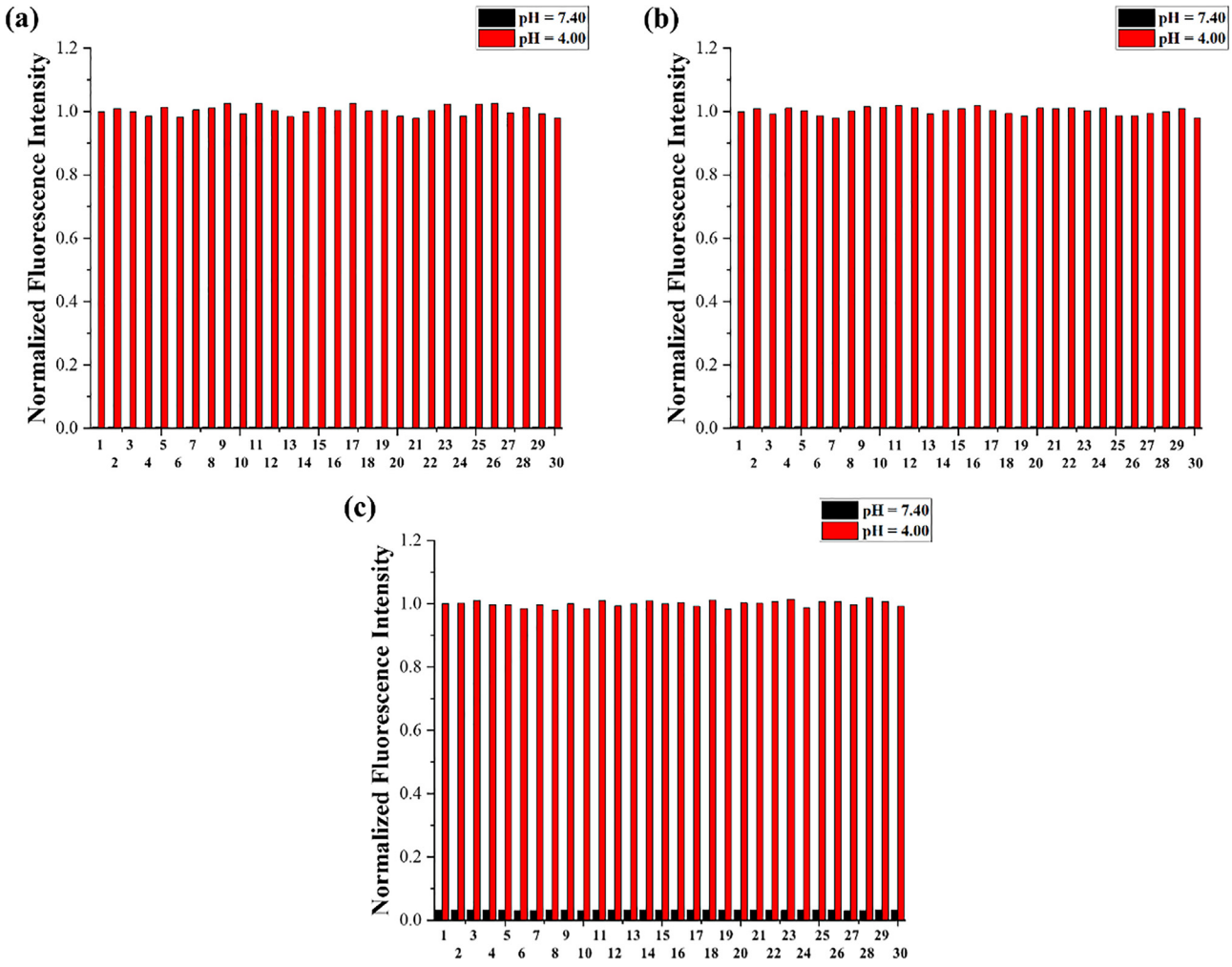

Fig. 3. Fluorescence responses of 5 μM (a) **RLH A**, (b) **RLH B** and (c) **RLH C** to different interferents in pH 4.00 and 7.40 BR buffer solutions: (1) control; (2) Na^+; (3) K^+; (4) Ca^{2+}; (5) Mg^{2+}; (6) Cd^{2+}; (7) Co^{2+}; (8) Ni^{2+}; (9) Zn^{2+}; (10) Cu^{2+}; (11) Fe^{3+}; (12) Ac^-; (13) NO_3^-; (14) SO_3^{2-}; (15) SO_4^{2-}; (16) HS^-; (17) HCO_3^-; (18) CO_3^{2-}; (19) Cys; (20) Ser; (21) Arg; (22) Met; (23) Lys; (24) Thr; (25) Leu; (26) Trp; (27) Glu; (28) His; (29) Asp; (30) GSH.

simplified the sensing process and proposed the reaction path in Scheme 2 according to previous reports [38–40]. The occurrence of the final amide rotation was subjected to the relative stability of **O2** and **O3**. The final protonated products were named **RLH**

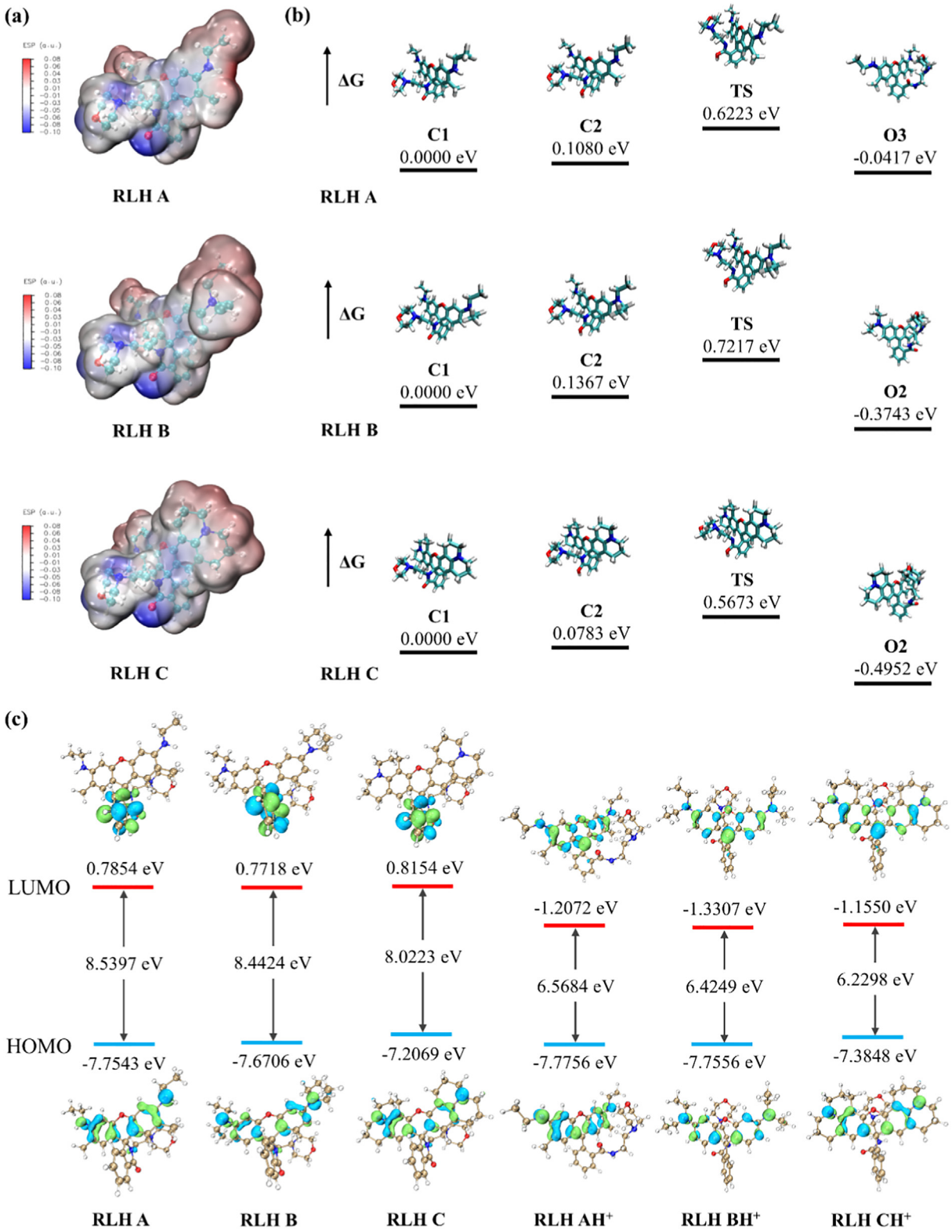

Fig. 4. (a) Electrostatic potential surfaces of **RLH A-C**; (b) Relative Gibbs free energy of representative states of **RLH A-C** in ring-opening process; (c) computed frontier orbitals and energy levels of **RLH A-C** and their proton versions **RLH A-CH$^+$**.

AH$^+$, **RLH BH$^+$** and **RLH CH$^+$**, which featured open spirolactam arrangements.

Liu and Xu described the spirocyclization equilibrium of rhodamine with the Gibbs free energy differences between the closed and open forms ($\Delta G_{C\text{-}O}$) and applied to spontaneously blinking rhodamines designing [41,42]. Inspired by these pioneer works, we tried to connected pK_a with the corresponding $\Delta G_{O\text{-}C}$. As shown in Table 1 and Fig. 4b, $\Delta G_{C\text{-}O}$ of **RLH A-C** were calculated as −0.0417, −0.3743 and −0.4952 eV respectively, which was negatively correlated with pK_a values. The transformation of **C2** to **O1**

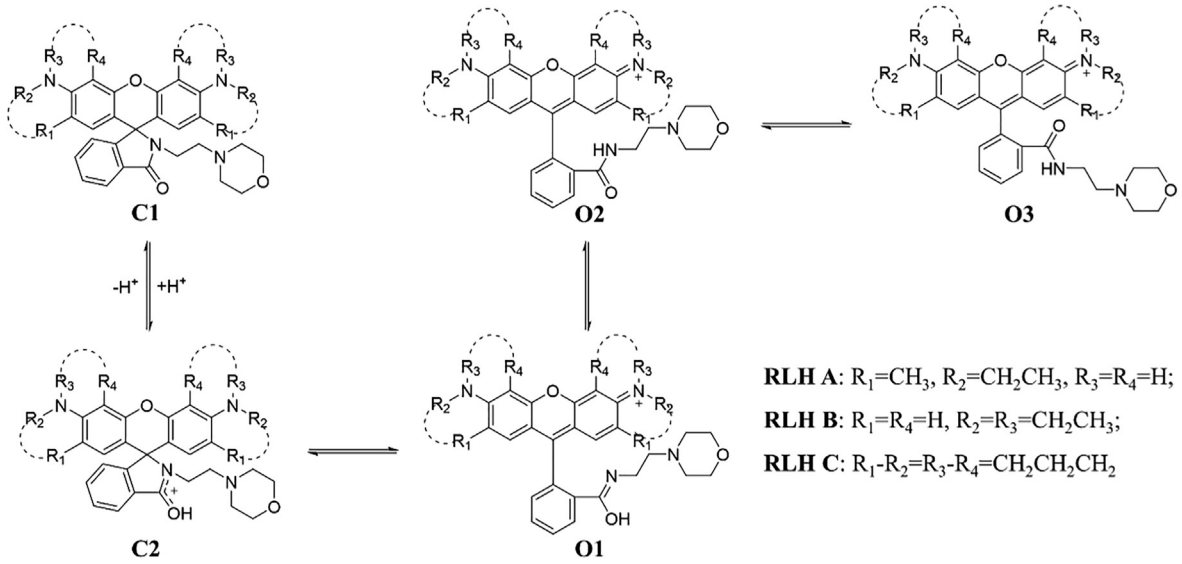

Scheme 2. The ring-opening process of **RLH A-C** during acid-activation.

was the rate-determining step in the ring-opening process because it was the only step that involves the breaking of chemical bonds [40]. According to the transition-state theory, the larger ΔG_{TS} resulted slower reaction rate. We then calculated the energy barrier ΔG_{TS} of the ring-opening reaction of **RLH A-C** (Table 1 and Fig. 4b). Our results showed **RLH B** exhibited the highest energy barrier (0.5850 eV) followed by **RLH A** (0.5143 eV) and **RLH C** (0.4890 eV) from **C2** to **O1**, which was also negatively correlated with k_{obs} values.

As presented in optimized geometries of the probes (Tables S1-7, S10-16 and S19-25), the torsion angles between xanthenyl ring and pendent ring were greatly increased from **RLH A-C** to their protonated versions **RLH AH$^+$–CH$^+$**. The specific increase in angle labeled C1-C2-O9 ranged from 140.33 to 179.55, 140.80–179.56 and 142.90–178.24^0, respectively. Besides, the selected atoms list in Tables S7, S16 and S25 revealed shorter distances upon protonation, which indicated the probes became more conjugated during the ring-opening reaction.

Electronic transition maxima of **RLH A-C** were calculated at 218, 220 and 224 nm, respectively (Fig. S14, S18 and S22). The ring-opening induced by acid shifted the transition to visible range and calculated to be 439, 455 and 475 nm for **RLH A-CH$^+$** respectively (Fig. S15, S19 and S23). In terms of fluorescence calculation, **RLH A-CH$^+$** presented the emission maximum at 511, 523 and 555 nm (Fig. S16, S20 and S24). These results were in reasonable agreement with the experimental data.

As shown in Fig. 4c, the HOMO and LUMO of **RLH A-C** were localized respectively on the xanthenyl ring and the spiro ring. Whereas in their pronated version **RLH A-CH$^+$**, the HOMO and LUMO both localized on the xanthenyl ring, which facilitate the electronic transition and lead to strong fluorescence. Besides, the decrease in HOMO-LUMO energy gaps from **RLH A-C** to **RLH A-CH$^+$** supported the red-shift of the absorption spectra during ring-opening reaction.

3.6. Applications in cellular imaging

We investigated the potential application of **RLH A-C** for fluorescence imaging of acidic microenvironment in HuH-7 cells. After incubating the cells with **RLH A** and Hoechst 33342, we only observed the fluorescence of Hoechst 33342 in nucleus under the excitation of 405 nm. Whereas, the fluorescence corresponded to **RLH A** under the excitation of 488 nm were observed outside the nucleus. Similarly, we could also find the fluorescence of **RLH B** and **RLH C** in the same position under the excitation of 561 nm (Fig. 5a). The fluorescence of **RLH C** was much brighter than **RLH A** and **RLH B**, which was attributed to the higher pK_a value. Besides, the most rapid reaction rate to protons further indicated **RLH C** was superior to the other two probes in imaging acidic microenvironment. Considering the acidity in lysosome, we anticipated that **RLH C** could selectively target lysosomes in cells. The co-localization analysis of **RLH C** and Lyso Tracker Green DND-26 with Pearson's coefficient of 0.96 indicated **RLH C** selectively stains lysosomes in live cells (Fig. 5b). The excellent spectral and pH response features of **RLH C** prompted us to further investigate the ability of it to monitor the pH fluctuations in living cells. HuH-7 cells were incubated with different pH PBS buffers in the presence of 10 μM nigericin to equilibrate the intracellular pH with external media. As shown in Fig 6c, the fluorescence intensity of **RLH C** decreased with the pH increased from 4.00 to 8.00. This trend was in perfect agreement with the *in vitro* result.

4. Conclusions

In summary, we have constructed spirolactam based pH probes (**RLH A-C**) with three common rhodamines. After measured the spectroscopic responses to pH, we determined the pK_a values and the observed rate constant k_{obs} of **RLH A-C**. These results were negatively correlated with calculated $\Delta G_{C\text{-}O}$ and ΔG_{TS} respectively. Besides, the spectra properties were also coincident with the computational results. The highest pK_a value and reaction rate resulted **RLH C** was superior to the other two probes in selectively imaging lysosomes. These results in our research might facilitate the quantitative optimization of rhodamine spirolactam based fluorescent probes.

CRediT authorship contribution statement

Fei Deng: Conceptualization, Investigation, Writing – original draft. **Dongsheng Sun:** Investigation, Validation. **Shixu Yang:** Investigation, Validation. **Wei Huang:** Formal analysis, Visualization. **Chunfang Huang:** Formal analysis, Data curation. **Zhaochao Xu:** Writing – review & editing. **Limin Liu:** Funding acquisition, Supervision.

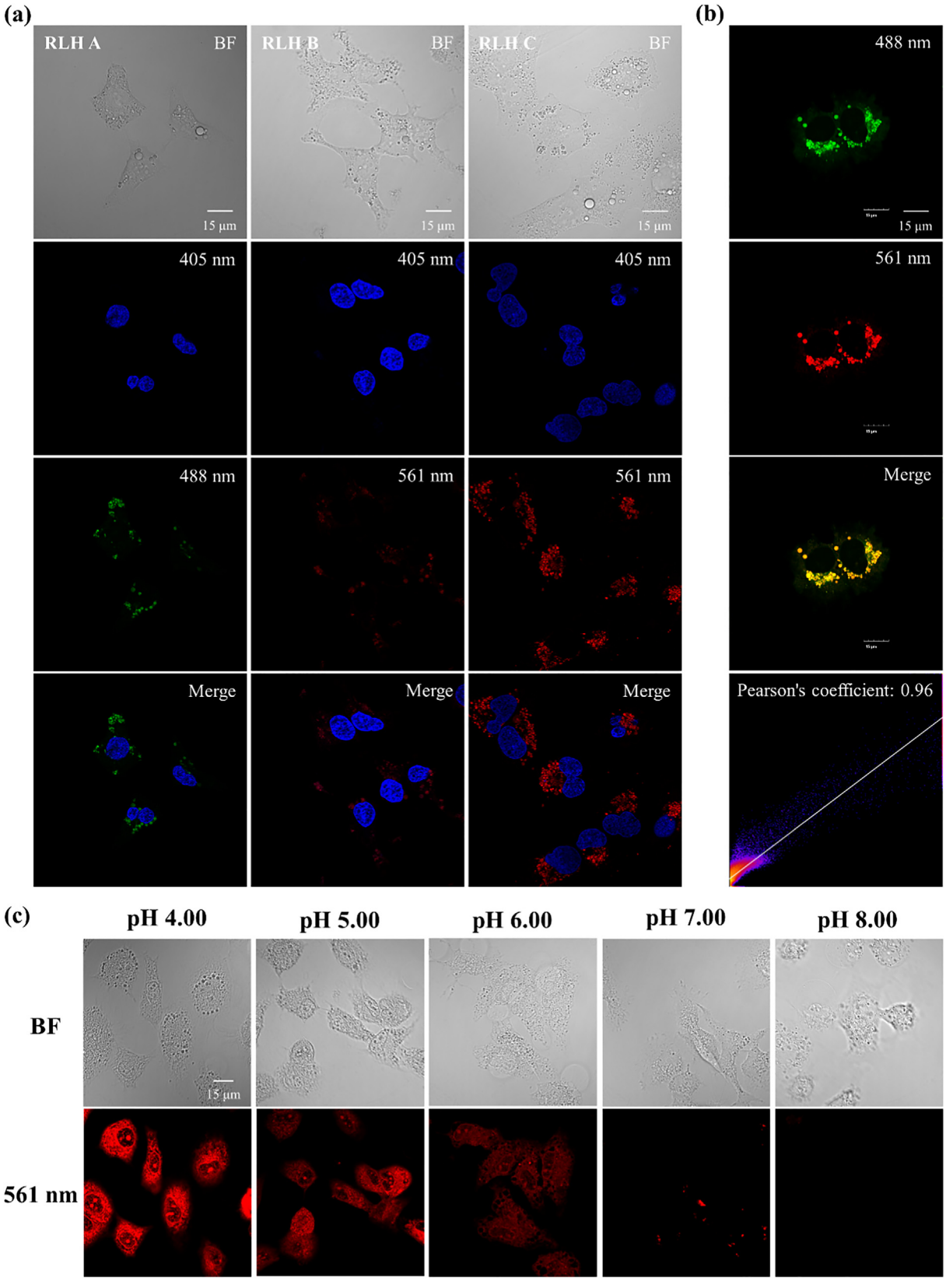

Fig. 5. (a) Confocal images of HuH-7 cells stained with Hoechst 33342 and **RLH A-C**; (b) Co-localization images of HuH-7 cells stained with Lyso Tracker Green DND-26 and **RLH C**; (c) Confocal images of HuH-7 cells in different pH PBS buffers stained with **RLH C**.

Declaration of Competing Interest

The authors declare that they have no known competing financial interests or personal relationships that could have appeared to influence the work reported in this paper.

Acknowledgment

We acknowledge the financial support from National Natural Science Foundation of China (21765011), Jiangxi Provincial Natural Science Foundation (20202BABL213008) and Jiangxi Provincial Department of Education, China (GJJ190567, GJJ201029).

Appendix A. Supplementary material

Supplementary data to this article can be found online at https://doi.org/10.1016/j.saa.2021.120662.

References

[1] K.J. Anson, G.A. Corbet, A.E. Palmer, Zn^{2+} influx activates ERK and Akt signaling pathways, Proc. Natl. Acad. Sci. U.S.A. 118 (2021) e2015786118
[2] Z. Zhou, H. Wu, R. Yang, A. Xu, Q. Zhang, J. Dong, C. Qian, M. Sun, GSH depletion liposome adjuvant for augmenting the photothermal immunotherapy of breast cancer, Sci. Adv. 6 (2020) eabc4373.
[3] E.L. Que, R. Bleher, F.E. Duncan, B.Y. Kong, S.C. Gleber, S. Vogt, S.i. Chen, S.A. Garwin, A.R. Bayer, V.P. Dravid, T.K. Woodruff, T.V. O'Halloran, Quantitative mapping of zinc fluxes in the mammalian egg reveals the origin of fertilization-induced zinc sparks, Nat. Chem. 7 (2) (2015) 130–139.
[4] Z. Liu, X. Zhou, Y.u. Miao, Y. Hu, N. Kwon, X. Wu, J. Yoon, A reversible fluorescent probe for real-time quantitative monitoring of cellular glutathione, Angew. Chem. Int. Edit. 56 (21) (2017) 5812–5816.
[5] Z. Wu, M. Liu, Z. Liu, Y. Tian, Real-time imaging and simultaneous quantification of mitochondrial H_2O_2 and ATP in neurons with a single two-photon fluorescence-lifetime-based probe, J. Am. Chem. Soc. 142 (16) (2020) 7532–7541.
[6] M. Vendrell, D. Zhai, J.C. Er, Y.-T. Chang, Combinatorial strategies in fluorescent probe development, Chem. Rev. 112 (8) (2012) 4391–4420.
[7] Z. Xu, J. Yoon, D.R. Spring, Fluorescent chemosensors for Zn^{2+}, Chem. Soc. Rev. 39 (6) (2010).
[8] K. Numasawa, K. Hanaoka, T. Ikeno, H. Echizen, T. Ishikawa, M. Morimoto, T. Komatsu, T. Ueno, Y. Ikegaya, T. Nagano, Y. Urano, A cytosolically localized far-red to near-infrared rhodamine-based fluorescent probe for calcium ions, Analyst 145 (23) (2020) 7736–7740.
[9] X. Li, H. Wang, Y. Zhang, Q. Cao, Y. Chen, A GSH-responsive PET-based fluorescent probe for cancer cells imaging, Chin. Chem. Lett. 32 (4) (2021) 1541–1544.
[10] V. Dujols, F. Ford, A.W. Czarnik, A long-wavelength fluorescent chemodosimeter selective for Cu(II) ion in water, J. Am. Chem. Soc. 119 (31) (1997) 7386–7387.
[11] M. Beija, C.A.M. Afonso, J.M.G. Martinho, Synthesis and applications of rhodamine derivatives as fluorescent probes, Chem. Soc. Rev. 38 (8) (2009) 2410, https://doi.org/10.1039/b901612k.
[12] X. Chen, T. Pradhan, F. Wang, J.S. Kim, J. Yoon, Fluorescent chemosensors based on spiroring-opening of xanthenes and related derivatives, Chem. Rev. 112 (3) (2012) 1910–1956.
[13] H.N. Kim, M.H. Lee, H.J. Kim, J.S. Kim, J. Yoon, A new trend in rhodamine-based chemosensors: application of spirolactam ring-opening to sensing ions, Chem. Soc. Rev. 37 (2008) 1465–1472.
[14] D. Ren, Y. Liu, X. Liu, Z. Li, H. Li, X.-F. Yang, Spirohydrazine rhodamine as a fluorescent chemodosimeter for the selective detection of Cu(II) ions and its application in live cell imaging, Sensor Actuat. B-Chem. 255 (2018) 2321–2328.
[15] J. Wan, K. Zhang, C. Li, Y. Li, S. Niu, A novel fluorescent chemosensor based on a rhodamine 6G derivative for the detection of Pb^{2+} ion, Sensor Actuat. B-Chem. 246 (2017) 696–702.
[16] P. Xie, Y. Zhu, X. Huang, G. Gao, F. Wei, F. Guo, S. Jiang, C. Wang, A novel probe based on rhodamine 101 spirolactam and 2-(2'-hydroxy-5'-methylphenyl) benzothiazole moieties for three-in-one detection of paramagnetic Cu^{2+}, Co^{2+} and Ni^{2+}, Spectrochim. Acta A 222 (2019) 117171.
[17] S.L. Shen, X.F. Zhang, Y.Q. Ge, Y. Zhu, X.Q. Lang, X.Q. Cao, A near-infrared lysosomal pH probe based on rhodamine derivative, Sensor Actuat. B-Chem. 256 (2018) 261–267.
[18] Y. Zhang, S. Xia, M. Fang, W. Mazi, Y. Zeng, T. Johnston, A. Pap, R.L. Luck, H. Liu, New near-infrared rhodamine dyes with large stokes shifts for sensitive sensing of intracellular pH changes and fluctuations, Chem. Commun. 54 (55) (2018) 7625–7628.
[19] F. Deng, L. Liu, W. Huang, C. Huang, Q. Qiao, Z. Xu, Systematic study of synthesizing various heteroatom-substituted rhodamines from diaryl ether analogues, Spectrochim. Acta A 240 (2020) 118466.
[20] W. Zhou, X. Fang, Q. Qiao, W. Jiang, Y. Zhang, Z. Xu, Quantitative assessment of rhodamine spectra, Chin. Chem. Lett. 32 (2) (2021) 943–946.
[21] H. Zheng, G.-Q. Shang, S.-Y. Yang, X. Gao, J.-G. Xu, Fluorogenic and chromogenic rhodamine spirolactam based probe for nitric oxide by spiro ring opening reaction, Org. Lett. 10 (12) (2008) 2357–2360.
[22] B. Wang, S. Yu, X. Chai, T. Li, Q. Wu, T. Wang, A lysosome-compatible near-infrared fluorescent probe for targeted monitoring of nitric oxide, Chem. Eur. J. 22 (16) (2016) 5649–5656.
[23] Y. Huo, J. Miao, L. Han, Y. Li, Z. Li, Y. Shi, W. Guo, Selective and sensitive visualization of endogenous nitric oxide in living cells and animals by a sirhodamine deoxylactam-based near-infrared fluorescent probe, Chem. Sci. 8 (10) (2017) 6857–6864.
[24] T. Wang, Q.J. Zhao, H.G. Hu, S.C. Yu, X. Liu, L. Liu, Q.Y. Wu, Spirolactonized Si-rhodamine: a novel NIR fluorophore utilized as a platform to construct Si-rhodamine-based probes, Chem. Commun. 48 (2012) 8781–8783.
[25] X.-L. Shi, G.-J. Mao, X.-B. Zhang, H.-W. Liu, Y.-J. Gong, Y.-X. Wu, L.-Y. Zhou, J. Zhang, W. Tan, Rhodamine-based fluorescent probe for direct bio-imaging of lysosomal pH changes, Talanta 130 (2014) 356–362.
[26] G. Niu, P. Zhang, W. Liu, M. Wang, H. Zhang, J. Wu, L. Zhang, P. Wang, Near-infrared probe based on rhodamine derivative for highly sensitive and selective lysosomal pH tracking, Anal. Chem. 89 (3) (2017) 1922–1929.
[27] X.F. Zhang, T.R. Wang, X.Q. Cao, S.L. Shen, A near-infrared rhodamine-based lysosomal pH probe and its application in lysosomal pH rise during heat shock, Spectrochim. Acta A 227 (2020) 117761.
[28] X. Chen, S.-W. Nam, M.J. Jou, Y. Kim, S.-J. Kim, S. Park, J. Yoon, Hg^{2+} selective fluorescent and colorimetric sensor: its crystal structure and application to bioimaging, Org. Lett. 10 (2008) 5235–5238.
[29] S. Grimme, A. Hansen, S. Ehlert, J.-M. Mewes, r^2SCAN-3c: a "Swiss army knife" composite electronic-structure method, J. Chem. Phys. 154 (2021) 064103.
[30] F. Neese, The ORCA program system, WIREs Comput. Mol. Sci. 2 (1) (2012) 73–78.
[31] F. Neese, Software update: the ORCA program system, version 4.0, WIREs Comput. Mol. Sci. 8 (2018) e1327.
[32] F. Neese, F. Wennmohs, U. Becker, C. Riplinger, The ORCA quantum chemistry program package, J. Chem. Phys. 152 (2020) 224108.
[33] C.-G. Zhan, D.A. Dixon, Absolute hydration free energy of the proton from first-principles electronic structure calculations, J. Phys. Chem. A 105 (51) (2001) 11534–11540.
[34] T. Lu, F. Chen, Multiwfn: a multifunctional wavefunction analyzer, J. Comput. Chem. 33 (2012) 580–592.
[35] W. Humphrey, A. Dalke, K. Schulten, VMD: visual molecular dynamics, J. Mol. Graph. 14 (1996) 33–38.
[36] M.D. Hanwell, D.E. Curtis, D.C. Lonie, T. Vandermeersch, E. Zurek, G.R. Hutchison, Avogadro: an advanced semantic chemical editor, visualization, and analysis platform, J. Cheminform. 4 (2012) 1–17.
[37] F. Deng, Q. Qiao, J. Li, W. Yin, L.u. Miao, X. Liu, Z. Xu, Multiple factors regulate the spirocyclization equilibrium of Si-rhodamines, J. Phys. Chem. B 124 (34) (2020) 7467–7474.
[38] S. Xia, M. Fang, J. Wang, J. Bi, W. Mazi, Y. Zhang, R.L. Luck, H. Liu, Near-infrared fluorescent probes with BODIPY donors and rhodamine and merocyanine acceptors for ratiometric determination of lysosomal pH variance, Sensor Actuat. B-Chem. 294 (2019) 1–13.
[39] S.G. Stratton, G.H. Taumoefolau, G.E. Purnell, M. Rasooly, W.L. Czaplyski, E.J. Harbron, Tuning the pK_a of fluorescent rhodamine pH probes through substituent effects, Chem. Eur. J. 23 (56) (2017) 14064–14072.
[40] Q. Qi, W. Chi, Y. Li, Q. Qiao, J. Chen, L.u. Miao, Y.i. Zhang, J. Li, W. Ji, T. Xu, X. Liu, J. Yoon, Z. Xu, A H-bond strategy to develop acid-resistant photoswitchable rhodamine spirolactams for super-resolution single-molecule localization microscopy, Chem. Sci. 10 (18) (2019) 4914–4922.
[41] W. Chi, Q. Qiao, C. Wang, J. Zheng, W. Zhou, N. Xu, X. Wu, X. Jiang, D. Tan, Z. Xu, X. Liu, Descriptor $\Delta G_{C\text{-}O}$ enables the quantitative design of spontaneously blinking rhodamines for live-cell super-resolution imaging, Angew. Chem. Int. Edit. 59 (45) (2020) 20215–20223.
[42] W. Chi, Q. Qi, R. Lee, Z. Xu, X. Liu, A unified push-pull model for understanding the ring-opening mechanism of rhodamine dyes, J. Phys. Chem. C 124 (6) (2020) 3793–3801.